Research Article Vol. 3, No. 7 / 15 July 2020 / OSA Continuum 1826

Continuous-wave terahertz emitter with hybrid nanoelectrodes based on graphene and nanowire

ALAA JABBAR JUMAAH,[1,3] SHIHAB AL-DAFFAIE,[1,2,4] OKTAY YILMAZOGLU,[1] AND THOMAS KUSSEROW[1]

[1] *Institute for Microwave Engineering and Photonics, Technical University of Darmstadt, Germany*
[2] *Terahertz Photonic Systems, Department of Electrical Engineering, TU Eindhoven, Eindhoven, The Netherlands*
[3] *jumaah@imp.tu-darmstadt.de*
[4] *shihab@imp.tu-darmstadt.de*

Abstract: Continuous-wave terahertz emitters based on photomixers with hybrid nanoelectrodes are investigated. The nanoelectrodes consist of a nitrogen-doped single layer of graphene and silver nanowires, placed on low-temperature-grown (LTG) GaAs as photoconductive material. Due to the high transparency of graphene and the low fill factor of nanowire nanoelectrodes, high photocurrents in the range from 260 μA to 1.8 mA can be reached. Despite their very small size nanoelectrodes provide the capability of handling rather high currents, leading to THz output signals reasonably three times higher than for conventional interdigitated finger electrodes for the whole measurement range. Measurement results of generated photocurrents and THz output signals are presented, showing the increased performance of our approach while maintaining highly reliable operation of the devices.

1. Introduction

Terahertz (THz) radiation sources are essential requirements for many applications in the fields of biology, physics, chemistry, medicine, materials spectroscopy, security [1–7], and many other application fields. A continuous-wave (CW) THz source is far superior to its pulsed competitor in terms of its high-frequency resolution, low-cost as well as compactness. Many efforts have been made within the last decade to fabricate and improve THz devices with high cut-off frequencies of up to several THz at room temperature operation [8–10]. One of the main reliable CW THz sources for highly tunable operation is the photomixer [11]. Conventional lateral photomixers use metal electrodes on a planar high-speed photoconductive material such as LTG-GaAs. The THz wave is generated by an optical heterodyne down-conversion using two detuned distributed feedback laser diodes (DFB-LDs) [12]. The intensity of the result interference signal is modulated with a frequency Δf corresponding to the frequency difference between the two optical laser sources. The resulted beat signal is used to illuminate the active region around the metal electrodes to generate electrons and holes in the semiconductor periodically. The electrons and holes are separated by an external field due to a DC bias. The resulting photocurrent contains a THz component due to the periodic modulation of the carrier generation rate [11,13]. The high frequency wave can be directly coupled from the photoconductive material into a suitable antenna for THz radiation. These conventional lateral photomixers have limitations regarding to bias voltage, optical beat signal power, reliability at high photocurrents, and the effective local heat dissipation which reduces the THz output power (PTHz) [13]. The output power is defined [14] as

$$P_{THz} = \frac{I_{ph}^2 R_A}{2[1 + (\omega\tau_c)^2][1 + (\omega R_A C)^2]} \tag{1}$$

#392837 https://doi.org/10.1364/OSAC.392837
Journal © 2020 Received 17 Mar 2020; revised 29 May 2020; accepted 29 May 2020; published 29 Jun 2020

OSA CONTINUUM

where $I_{ph} = V_{bias}G$ is the photocurrent, V_{bias} is bias voltage, G is the photoconductive gain, R_A is the antenna resistance, τ_c is the carrier life time, and C is the device capacitance. R_A is fixed for the chosen antenna design, and τ_c is constant for the grown LTG-GaAs material. Therefore, in order to increase the THz output power, the device capacity should be decreased and the photocurrent should be increased. The photocurrent is proportional to the photoconductive gain, which is the ratio between the number of electrons collected per unit time (N_{el}) and the number of absorbed photons per unit time (N_{ph}) [15],

$$G = \frac{N_{el}}{N_{ph}} = \frac{J_{ph}A_c / e}{P_{abs} / \hbar\omega} \tag{2}$$

where A_C is the cross-sectional area of the device, e is the charge unit, $\hbar\omega$ is the photon energy, P_{abs} is the optical power absorbed by the device, and J_{ph} is the photocurrent density. Therefore, transparent materials are required to increase the effective illuminated area, and increase the number of photogenerated carriers which results in increased photocurrent, and higher THz output power.

Nowadays, nanomaterials, such as NWs [16–18] and graphene [19–22] demonstrate new enhanced functions crucial to many areas of technology. Recently, silver (Ag) NWs based THz photomixers have shown an enhanced emission particularly at higher frequencies (>1 *THz*) compared to conventional photomixer with interdigitated finger design [23]. These Ag-NWs based THz photomixers have shown approximately one order of magnitude reduction of the device capacitance due to the low fill factor (small contact area) in the active region of the photomixer. Later, it has been shown by direct near-field observation on Ag-NWs that further enhancement of the Ag-NWs THz photomixers can be attributed to surface plasmon polaritons (SPP) which can be generated by a linearly polarized light incident at the end of a nanowire [24]. The atomically smooth surface of the Ag-NWs allows the overall propagation loss to be much lower than for other materials. However, The light coupling for plasmon excitation into such small structures remains a practical issue [25]. Furthermore, due to the small contact area, the contribution of photogenerated carriers, which are generated far from the nanowire will be lost. In a similar way as NWs, graphene is currently drawing exceptional attention for EM applications at the microwave, terahertz (THz), and optical frequencies due to its unique electronic and optical properties [26]. It has high thermal and electrical conductivity, and high intrinsic mobility, which makes graphene a very promising material for transparent conductive electrodes [23,27–29], among many other potential applications. Accordingly to the conductivity of graphene, it has been recently shown that the lateral confinement of electrons in graphene enhances the material conductivity in the THz band [30,31]. The propagation of SPP waves on graphene has been recently analytically studied and experimentally shown [32–35]. SPP waves on graphene have been observed at THz frequencies and these SPP can be tuned through material doping. Moreover, the high transparency of graphene allows almost all the optical light to propagate through graphene, which allows higher photogenerated carrier densities [26]. Additionally, the lateral heat dissipation is improved due to the thermal conductivity of the graphene from the small active area to the large antenna structure, which increases the device stability [36]. The combined use of Ag-NW and graphene enhances the performance of the device as reported in [37–39], which makes them a very promising material as a hybrid nanoelectrodes for THz photomixer devices. The combination of graphene and NW has been recently explored, where NWs with low fill factor can improve their own conductive paths by the conductivity of graphene. In this approach, the graphene flakes act as local recombination centers, subsequently, they will reduce the mean-free path of the photocarriers and hence, reducing carrier lifetimes. Moreover, the plasmonic effect close to the graphene flakes forms rich sources of photogenerated carriers, resulting in high drift current densities. On the other hand, the SPP of the Ag-NW allows capturing the high drifted current densities and serves as a highly capable transport

OSA CONTINUUM

medium for the high current densities. Therefore, both conductive components based on graphene and the NW allow simultaneous charge transport in the hybrid nanostructure, where each part complements the disadvantages of the other component [38]. In this article, an Ag-NW and nitrogen-doped single-layer graphene flakes (lateral size 0.5-5 μm, obtained from ACS Material LLC.) were combined as hybrid nanoelectrodes for a CW THz photomixer. Due to the small size of the graphene flakes, the light will be confined around the graphene flakes. This light confinement will enhance the electric field between the graphene flakes. Therefore, we assume that the photogenerated carriers will be transported between these flakes by a spatial plasmonic field, and this makes the graphene flakes act as connected rather than isolated. Finally, these carries are drifted to the Ag-NW. Therefore, the conductivity of the NWs, in spite of its low fill factor, has improved by the conductivity of the graphene. Additionally, due to the high transparency for the graphene, the optical beat signal propagates through graphene to generate more carriers. The performance of the enhanced photomixer was compared with a conventional photomixer with interdigitated finger electrodes.

2. Fabrication and Measurement

First, a log-periodic antenna was designed with the size ratio of tooth/anti-tooth = 0.707, the ratio of the radial sizes of successive teeth = 0.5, and the gap width between the antenna contacts = 10 μm [40]. Then, Ni(25 nm)/Au(150 nm) was evaporated on top of LTG-GaAs wafer (thickness ~ 350 μm) to form the log-periodic antenna using a standard optical lithography process. Secondly, N^+SLG flakes were dispersed in ethanol with a dispersion aid [Sodium Dodecyl Benzene Sulfonate (SDBS)] with the properties 0.1 mg, 1 ml, and 10 mg, respectively. Thirdly, this dispersed graphene was mixed with Ag-NW (ϕ 300 nm). Few drops of the mixed solution were applied in the antenna gap to deposit the graphene flakes in random positions and nanowire was randomly aligned to perform as nanoelectrodes between the antenna contacts. Figures 1 and 2 show the schematic diagram and a microscope image of the photomixer with hybrid nanoelectrodes (N^+SLG/Ag-NW) on LTG-GaAs.

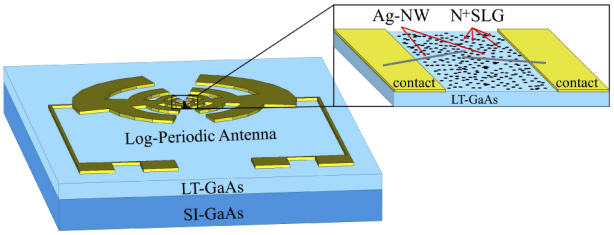

Fig. 1. Schematic diagram of the photomixer with hybrid electrodes (N^+SLG/Ag-NW) on LTG-GaAs.

For the characterization of the device, two tunable DFB-LDs (wavelength ~ 850 nm) were coupled by a 50 : 50 combiner to generate the beat signal. Afterwards, the beat signal was coupled into a cleaved polarization-maintaining (PM) optical fiber. The end of the fiber was aligned close to the chip surface in order to fully illuminate the 10×10 μm^2 active area by the optical beat signal. The photomixer chip was mounted on a hemispherical Si lens. The Si lens was used to couple and direct the THz radiation into two parabolic mirrors which are used to direct the THz beam. A DC power supply was implemented to accelerate the photogenerated carriers. The THz output signal was measured by using a Golay Cell Detector (GCD) with a lock-in amplifier as shown in Fig. 3.

OSA CONTINUUM

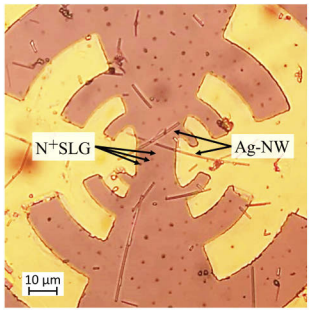

Fig. 2. Optical microscope image of the photomixer with hybrid electrodes (N^+SLG/Ag-NW) on LTG-GaAs.

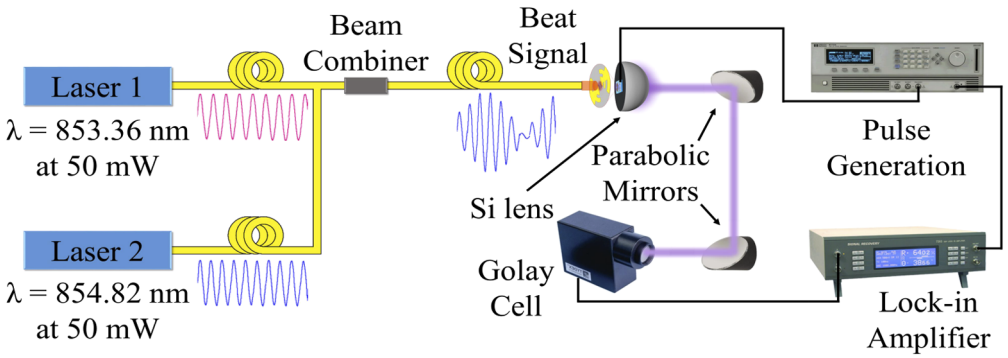

Fig. 3. Schematic representation of the setup for measuring the THz emission of the fabricated photomixer.

3. Measurement Results

The measurements are divided into two parts, the I-V characterization and the THz output power measurements for the photomixer with hybrid nanoelectrodes. These results were compared with a conventional photomixer with interdigitated metal finger electrodes. The measurements were performed under same conditions for both photomixers.

3.1. I-V Measurements

The active area of the photomixers was illuminated with a total optical power of 28 mW, while the bias voltage varied from 0-15 V. The initial I-V characterization of the photomixer with hybrid nanoelectrodes showed a highly reliable maximum photocurrent of ~ 1.8 mA, a small dark current of 90 nA, and an on/off ratio of more than four orders of magnitude as reported in [41]. The I-V measurement results were compared to a conventional photomixer with interdigitated metal finger electrodes using same conditions above. The conventional photomixer showed a maximum generated photocurrent of 260 μA before local heating damages the device at 15 V. The hybrid nanoelectrodes showed an increase of the maximum achievable photocurrent under reliable conditions by more than 7 times due to the improved conductivity. Figure 4 shows a comparison of the I-V characteristic between the photomixer with hybrid nanoelectrodes and the conventional interdigitated metal finger electrodes photomixer.

OSA CONTINUUM

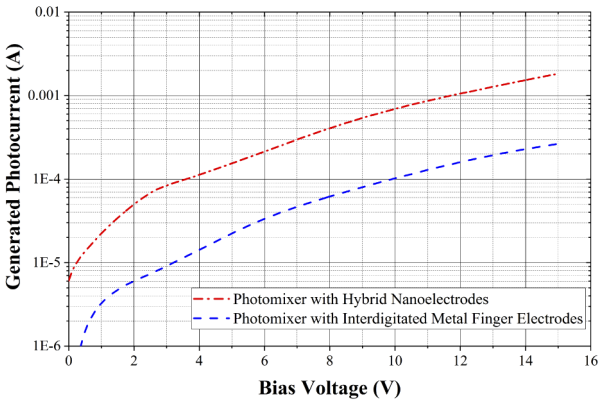

Fig. 4. Comparison of the DC characteristic between the photomixer with hybrid nanoelectrodes and the photomixer with 6-finger metal electrodes.

3.2. THz Power Measurements

Two slightly detuned DFB-LDs (wavelength ~ 850 *nm*) were used to generate the optical beat signal (P = 28 *mW*) with a beating frequency corresponding to the frequency difference between the two DFB-LDs. By changing the frequency difference between the two DFB-LDs, the range between 200 *GHz* and 1 *THz* was covered. A bias voltage of 14 *V* was chosen to accelerate the photogenerated carriers. The THz output radiation was transformed into an electrical signal using a GCD as shown in Fig. 5. A lock-in amplifier was used to extract the amplitude of the signal in terms of voltage. The THz output power is proportional to the measured voltage amplitude by a factor of R_v, where R_v is the responsivity of the detector. The voltage responsivity R_v of a photodetector [42] is

$$R_v = \eta \frac{q\lambda}{hc} \quad [kV/W] \tag{3}$$

where η is the quantum efficiency of the detector, q is the electron charge, λ is the incident light wavelength, h is Planck's constant, and c is the speed of light in vacuum.

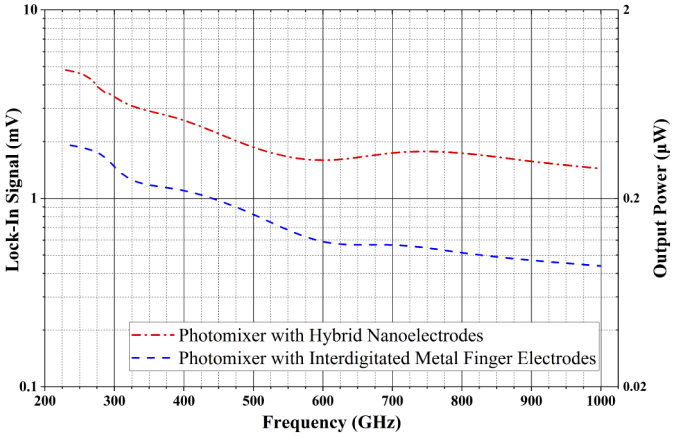

Fig. 5. Comparison of the relative output voltage measured from the photomixer with hybrid nanoelectrodes and the photomixer with 6-finger metal electrodes.

As expected from the results of the I-V measurements, a significant improvement is obtained in the THz measurement results due to the use of hybrid electrodes instead of the interdigitated metal

OSA CONTINUUM

finger electrodes. The lock-in signal level is clearly increased for the whole THz measurement range (see Fig. 5). The output power of the conventional interdigitated photomixer is decayed rapidly due to the high device capacitance. The effect of the low device capacitance of the hybrid nanoelectrodes photomixer results in high output power especially at high frequency.

Figure 6 shows how much the performance has been improved over the entire measurement range for THz photomixer by using graphene flakes and Ag-NW as hybrid nanoelectrodes instead of conventional metal electrodes. The output power of the hybrid nanoelectrodes based photomixer improved by a factor of two compared to the conventional interdigitated photomixer, in the high frequency range even more than three times higher output power levels were achieved. The increase in the relative THz output power allows for the photomixer to operate the THz source for much broader frequency ranges than that of the conventional interdigitated photomixer under the same antenna specifications. The output power of the hybrid nanoelectrodes photomixer can be further improved by carefully designing the nanoelectrodes to manage the high generated photocurrent and reduced the device capacitance. Additionally, a perfect impedance matching between the photomixer and the antenna results in highly improved performance.

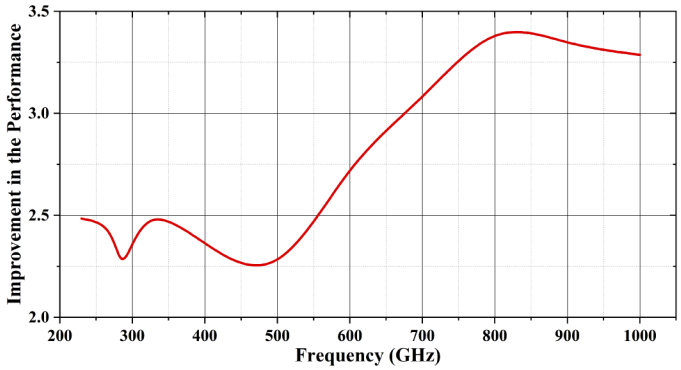

Fig. 6. The ratio of the performance of the photomixer with hybrid electrodes (N^+SLG/Ag-NW) and a conventional interdigitated photomixer over the whole spectral range of the measurement.

4. Conclusion

Hybrid nanoelectrodes consisting of Ag-NW and graphene on LTG-GaAs photomixer combine the benefits of graphene such as transparency and electrical conductivity with the benefits of the Ag-NW such as high conductivity and capability of handling higher current density without damaging the device. The new photomixer with hybrid nanoelectrodes showed 7 times higher photocurrent than the conventional photomixer with interdigitated metal finger electrodes. The increase in the generated photocurrent leads to an increase in the relative THz output power for the photomixer with hybrid nanoelectrodes by a factor of more than two at low frequencies and more than three times at high frequencies than the conventional interdigitated photomixer. This increase in the relative output power allows the new photomixer with a hybrid photomixer to operate for a broader range of frequencies. The enhancement in the generated photocurrent and measured THz signal can be attributed to the transparency of the graphene, which increases the illuminated area and improves the optical conversion efficiency. Besides the increased number of photogenerated carriers, the field enhancement between graphene flakes allowed the fast carrier drift to the Ag-NW. The small contact area of the NW electrodes leads to higher THz power and increased cut-off frequencies. Furthermore, NWs also provides the capability to handle higher currents without damaging the device.

OSA CONTINUUM

The small gaps distance between the graphene flakes and Ag-NWs are responsible for the high field enhancement associate with the high THz signal. Therefore, an optimized gap between the nanocomponents can result in higher field enhancements and higher THz signal powers.

Funding

German Research Foundation and the Open Access Publishing Fund of Technische Universität Darmstadt.

Acknowledgments

We gratefully acknowledge the financial support from Innovative Training Network Convergence of Electronics and Photonics Technologies for Enabling Terahertz Applications (ITN CELTA) under grant number 675683 of Call: H2020-MSCA-ITN-2015.5.2.

Disclosures

The authors declare no conflicts of interest.

References

1. K. Kawase, J.-i. Shikata, and H. Ito, "Terahertz wave parametric source," J. Phys. D: Appl. Phys. **35**(3), R1–R14 (2002).
2. P. H. Siegel, "Terahertz technology in biology and medicine," IEEE Trans. Microwave Theory Tech. **52**(10), 2438–2447 (2004).
3. B. Jin, C. Zhang, P. Wu, and S. Liu, "Recent progress of terahertz spectroscopy on medicine and biology in china," Terahertz Sci. Technol. **3**(4), 192–200 (2010).
4. S. Hunsche, M. Koch, I. Brener, and M. Nuss, "Thz near-field imaging," Opt. Commun. **150**(1-6), 22–26 (1998).
5. J. Bjarnason, T. Chan, A. Lee, M. Celis, and E. Brown, "Millimeter-wave, terahertz, and mid-infrared transmission-through common clothing," Appl. Phys. Lett. **85**(4), 519–521 (2004).
6. T. Kleine-Ostmann, P. Knobloch, M. Koch, S. Hoffmann, M. Breede, M. Hofmann, G. Hein, K. Pierz, M. Sperling, and K. Donhuijsen, "Continuous-wave thz imaging," Electron. Lett. **37**(24), 1461–1463 (2001).
7. H.-B. Liu, H. Zhong, N. Karpowicz, Y. Chen, and X.-C. Zhang, "Terahertz spectroscopy and imaging for defense and security applications," Proc. IEEE **95**(8), 1514–1527 (2007).
8. E. Brown, K. McIntosh, K. Nichols, and C. Dennis, "Photomixing up to 3.8 thz in low-temperature-grown gaas," Appl. Phys. Lett. **66**(3), 285–287 (1995).
9. G. Scalari, C. Walther, M. Fischer, R. Terazzi, H. Beere, D. Ritchie, and J. Faist, "Thz and sub-thz quantum cascade lasers," Laser Photonics Rev. **3**(1-2), 45–66 (2009).
10. A. Maestrini, J. Ward, J. Gill, H. Javadi, E. Schlecht, G. Chattopadhyay, F. Maiwald, N. R. Erickson, and I. Mehdi, "A 1.7-1.9 thz local oscillator source," IEEE Microw. Wireless Compon. Lett. **14**(6), 253–255 (2004).
11. S. Preu, G. Döhler, S. Malzer, L. Wang, and A. Gossard, "Tunable, continuous-wave terahertz photomixer sources and applications," J. Appl. Phys. **109**(6), 061301 (2011).
12. G. Carelli, A. Moretti, D. Pereira, and F. Strumia, "Heterodyne frequency measurements of fir laser lines around 1.2 and 1.6 thz," IEEE J. Quantum Electron. **31**(1), 144–147 (1995).
13. S. Verghese, K. McIntosh, and E. Brown, "Optical and terahertz power limits in the low-temperature-grown gaas photomixers," Appl. Phys. Lett. **71**(19), 2743–2745 (1997).
14. E. Brown, F. Smith, and K. McIntosh, "Coherent millimeter-wave generation by heterodyne conversion in low-temperature-grown gaas photoconductors," J. Appl. Phys. **73**(3), 1480–1484 (1993).
15. Y. Dan, X. Zhao, K. Chen, and A. Mesli, "A photoconductor intrinsically has no gain," ACS Photonics **5**(10), 4111–4116 (2018).
16. Y. Wu, J. Xiang, C. Yang, W. Lu, and C. M. Lieber, "Single-crystal metallic nanowires and metal/semiconductor nanowire heterostructures," Nature **430**(6995), 61–65 (2004).
17. S. De, T. M. Higgins, P. E. Lyons, E. M. Doherty, P. N. Nirmalraj, W. J. Blau, J. J. Boland, and J. N. Coleman, "Silver nanowire networks as flexible, transparent, conducting films: extremely high dc to optical conductivity ratios," ACS Nano **3**(7), 1767–1774 (2009).
18. L. Hu, H. Wu, and Y. Cui, "Metal nanogrids, nanowires, and nanofibers for transparent electrodes," MRS Bull. **36**(10), 760–765 (2011).
19. P.-Y. Chen and A. Alu, "A terahertz photomixer based on plasmonic nanoantennas coupled to a graphene emitter," Nanotechnology **24**(45), 455202 (2013).
20. X. Luo, Y. Lee, A. Konar, T. Fang, H. Xing, G. Snider, and D. Jena, "Current-carrying capacity of long & short channel 2d graphene transistors," in *2008 Device Research Conference*, (IEEE, 2008), pp. 29–30.

OSA CONTINUUM

21. T. Otsuji, S. B. Tombet, A. Satou, H. Fukidome, M. Suemitsu, E. Sano, V. Popov, M. Ryzhii, and V. Ryzhii, "Graphene-based devices in terahertz science and technology," J. Phys. D: Appl. Phys. **45**(30), 303001 (2012).
22. X. Huang, Z. Zeng, Z. Fan, J. Liu, and H. Zhang, "Graphene-based electrodes," Adv. Mater. **24**(45), 5979–6004 (2012).
23. S. Al-Daffaie, O. Yilmazoglu, F. Küppers, and H. L. Hartnagel, "1-d and 2-d nanocontacts for reliable and efficient terahertz photomixers," IEEE Trans. Terahertz Sci. Technol. **5**(3), 398–405 (2015).
24. M. M. Wiecha, S. Al-Daffaie, A. Bogdanov, M. D. Thomson, O. Yilmazoglu, F. Küppers, A. Soltani, and H. G. Roskos, "Direct near-field observation of surface plasmon polaritons on silver nanowires," ACS Omega **4**(26), 21962–21966 (2019).
25. A. L. Pyayt, B. Wiley, Y. Xia, A. Chen, and L. Dalton, "Integration of photonic and silver nanowire plasmonic waveguides," Nat. Nanotechnol. **3**(11), 660–665 (2008).
26. P. Avouris, "Graphene: electronic and photonic properties and devices," Nano Lett. **10**(11), 4285–4294 (2010).
27. A. Jumaah, S. Al-Daffaie, O. Yilmazoglu, and F. Küppers, "Graphene enhanced 2-d nanoelectrode for continuous wave terahertz photomixers,", in *2018 43rd International Conference on Infrared, Millimeter, and Terahertz Waves (IRMMW-THz)*, (IEEE, 2018), pp. 1–2.
28. A. Jumaah, S. Al-Daffaie, O. Yilmazoglu, F. Küppers, and T. Kusserow, "Interdigital multilayer-graphene nanoelectrodes for continuous wave terahertz photomixers," in *2019 European Microwave Conference in Central Europe (EuMCE)*, (IEEE, 2019), pp. 265–267.
29. A. Jumaah, S. Al-Daffaie, O. Yilmazoglu, F. Küppers, and T. Kusserow, "Experimental investigation of graphene layers as 2d nanoelectrode for continuous wave terahertz generation," in *2019 44nd International Conference on Infrared, Millimeter, and Terahertz Waves (IRMMW-THz)*, (IEEE, 2019), pp. 1–2.
30. F. Hipolito, A. Chaves, R. Ribeiro, M. Vasilevskiy, V. M. Pereira, and N. Peres, "Enhanced optical dichroism of graphene nanoribbons," Phys. Rev. B **86**(11), 115430 (2012).
31. K.-i. Sasaki, K. Kato, Y. Tokura, K. Oguri, and T. Sogawa, "Theory of optical transitions in graphene nanoribbons," Phys. Rev. B **84**(8), 085458 (2011).
32. A. A. Dubinov, V. Y. Aleshkin, V. Mitin, T. Otsuji, and V. Ryzhii, "Terahertz surface plasmons in optically pumped graphene structures," J. Phys.: Condens. Matter **23**(14), 145302 (2011).
33. L. Ju, B. Geng, J. Horng, C. Girit, M. Martin, Z. Hao, H. A. Bechtel, X. Liang, A. Zettl, and Y. R. Shen, "Graphene plasmonics for tunable terahertz metamaterials," Nat. Nanotechnol. **6**(10), 630–634 (2011).
34. F. H. Koppens, D. E. Chang, and F. J. Garcia de Abajo, "Graphene plasmonics: a platform for strong light–matter interactions," Nano Lett. **11**(8), 3370–3377 (2011).
35. A. Y. Nikitin, F. Guinea, F. García-Vidal, and L. Martín-Moreno, "Edge and waveguide terahertz surface plasmon modes in graphene microribbons," Phys. Rev. B **84**(16), 161407 (2011).
36. I. N. Kholmanov, M. D. Stoller, J. Edgeworth, W. H. Lee, H. Li, J. Lee, C. Barnhart, J. R. Potts, R. Piner, D. Akinwande, J. E. Barrick, and R. S. Ruoff, "Nanostructured hybrid transparent conductive films with antibacterial properties," ACS Nano **6**(6), 5157–5163 (2012).
37. H. Lee, K. Heo, J. Park, Y. Park, S. Noh, K. S. Kim, C. Lee, B. H. Hong, J. Jian, and S. Hong, "Graphene–nanowire hybrid structures for high-performance photoconductive devices," J. Mater. Chem. **22**(17), 8372–8376 (2012).
38. M.-S. Lee, K. Lee, S.-Y. Kim, H. Lee, J. Park, K.-H. Choi, H.-K. Kim, D.-G. Kim, D.-Y. Lee, S. Nam, and J. Park, "High-performance, transparent, and stretchable electrodes using graphene–metal nanowire hybrid structures," Nano Lett. **13**(6), 2814–2821 (2013).
39. X. Huang, Z. Zeng, Z. Fan, J. Liu, and H. Zhang, "Graphene-based electrodes," Adv. Mater. **24**(45), 5979–6004 (2012).
40. R. Mendis, C. Sydlo, J. Sigmund, M. Feiginov, P. Meissner, and H. L. Hartnagel, "Tunable cw-thz system with a log-periodic photoconductive emitter," Solid-State Electron. **48**(10-11), 2041–2045 (2004).
41. A. Jumaah, S. Al-Daffaie, O. Yilmazoglu, and F. Küppers, "Graphene-nanowire hybrid photomixer for continuous-wave terahertz generation," in *2017 42nd International Conference on Infrared, Millimeter, and Terahertz Waves (IRMMW-THz)*, (IEEE, 2017), pp. 1–2.
42. J. Liu, C. Shan, B. Li, Z. Zhang, C. Yang, D. Shen, and X. Fan, "High responsivity ultraviolet photodetector realized via a carrier-trapping process," Appl. Phys. Lett. **97**(25), 251102 (2010).